Journal of Cleaner Production 423 (2023) 138832

Contents lists available at ScienceDirect

Journal of Cleaner Production

journal homepage: www.elsevier.com/locate/jclepro

Laboratory observations of solute transport in groundwater basins

Hong Niu [a], Jun-Zhi Wang [b,c,*], Sheng-Nan Ni [d], Xing Liang [e], Hong Du [a]

[a] Key Laboratory of Resources Conversion and Pollution Control of the State Ethnic Affairs Commission, College of Resources and Environmental Science, South-Central Minzu University, Hubei, Wuhan, 430074, China
[b] Yellow River Engineering Consulting Co., Ltd. (YREC), Henan, Zhengzhou, 450003, China
[c] Key Laboratory of Water Management and Water Security for Yellow River Basin, Ministry of Water Resources (under Construction), Henan, Zhengzhou, 450003, China
[d] College of Ship and Ocean, Naval University of Engineering, Hubei, Wuhan, 430033, China
[e] School of Environmental Studies, China University of Geosciences, Wuhan, 430074, China

ARTICLE INFO

Handling Editor: Jin-Kuk Kim

Keywords:
Groundwater flow systems
Step-input solute transport
Pulse-input solute transport
Residence time distributions

ABSTRACT

This paper introduces a method of groundwater pollution source identification obtained from laboratory by a physical instrument of Flow System Sand-Box Model. A Unit basin of a simple flow system and a Tóthian basin of a hierarchically nested flow structure are introduced as case studies. We add step-input solutes at recharge zones, separately or simultaneously, to obtain the breakthrough curves (BTCs) at each discharge zone. For the Unit basin, its BTC shows a gradual upward trend with a decreasing slope but with two more pronounced steps, which differs a lot from previous results of analytical and numerical solutions. These steps are caused by the settings of the current physical instrument as no solutes are input at the upper two discharge ports. For the Tóthian basin, internal steps may exist due to the late-time arrival of intermediate and regional groundwater flow systems. Although the Unit basin and Tóthian basin can both have internal steps in the BTCs, they are due to different reasons. By jointly solving solute mass balance equations with water mass balance equations, the circulation rate for each flow system is calculated, which quantitatively explains the phenomena encountered in the experiment and highlights the important contributions of intermediate and regional flow systems to the entire groundwater circulation. We indirectly obtain the pulse-input BTCs by deriving the step-input BTCs respective to time, which is also the residence time distribution (RTD) of the groundwater basin, that the groundwater pollution sources can be identified. The pulse-input BTC is characterized by peaks and sloping tails. The peaks correspond to the intermediate and regional groundwater flow systems. The sloping tails indicate the rate at which solutes are flushed out or contaminants fade away. By inputting tap water into the groundwater basin to purify the contaminations, we conduct self-purification experiments. The shapes of the solute-input curves and the self-purification curves are systematically symmetrical. As the self-purification experiment has less external interference, it is possible to use the self-purification curves to characterize and identify the groundwater flow system. This study proposes a physical method for identifying sources of groundwater contamination, and achieves a comprehensive understanding of the law of solute transport in groundwater basins, which could guide the prevention of non-point contamination at the basin scale.

1. Introduction

As the most active geological fluid, groundwater is not only an important component of the global water cycle (Alley et al., 2002), but also an active participant in various complex geological processes (Ingebritsen et al., 2006). At the basin scale, as illustrated by Tóth (1963a,b) and Haitjema and Mitchell-Bruker (2005), due to the undulation of water table and the variations of recharge to medium permeability, groundwater circulation could be extremely sophisticated of a hierarchically nested flow structure by local, intermediate, and regional flow systems. This flow structure can describe properly the groundwater circulation and evolution at the basin scale and is widely used in a series of geoscience fields such as geothermal exploitation, mineral and oil exploration, nuclear waste disposal, and eco-hydrology (Tóth, 1980, 2009).

In the literature, most of the studies on groundwater flow systems are

* Corresponding author. Yellow River Engineering Consulting Co., Ltd. (YREC), Henan, Zhengzhou, 450003, China.
E-mail address: nrg880607@126.com (J.-Z. Wang).

https://doi.org/10.1016/j.jclepro.2023.138832
Received 5 July 2023; Received in revised form 6 September 2023; Accepted 11 September 2023
Available online 13 September 2023

concerned with the characteristics of the hierarchically nested flow structure. To understand the influence of topography (Marklund and Wörman, 2011; Tóth, 1962, 1963; Tóth, 1963a,b; Wörman et al., 2007; Zijl, 1999), water table (Zhao et al., 2018; Zlotnik et al., 2015), infiltration recharge (Dai et al., 2021; Haitjema and Mitchell-Bruker, 2005; Liang et al., 2013; Xie et al., 2022; Zhang et al., 2022) and permeability (Freeze and Witherspoon, 1967; Jiang et al., 2009, 2011; Wang et al., 2011; Zlotnik et al., 2011) on the development of groundwater flow systems, methods such as analytical solutions, numerical simulations, and physical model experiments have been widely adopted based on an upper boundary of a specified head or a specified flux. Compared to methods of analytical and numerical simulations, although they may take up a lot of financial, material, and human resources, the physical model experiments are greatly helpful for our understanding complex concepts through direct observations (Simpson et al., 2003). Liang et al. (2010) found that young hydrogeologists often have difficulties in gaining intuitive insights into the theory of regional groundwater flow (Tóth, 2009), even if they may accept the concept with confirmations of analytical and numerical simulations. Therefore, Liang et al. (2010) developed a physical instrument of a complex Flow System Sand-Box Model, which enables the visual observations of the groundwater movement and the hierarchically nested flow structure in the laboratory.

As a ubiquitous and important geologic agent, groundwater interacts complicatedly with the surrounding geological environment during its circulating process (Tóth, 1980, 1999). In general, groundwater salinity, pH, hydrochemical composition, dissolved oxygen, etc., evolve regularly along the groundwater flow pathways under natural conditions. In the last few decades, due to the interference of human activities, a variety of contaminants, such as nutrients, pathogens, pesticides, and metals (USEPA, 2008) have been reported widespread across the world (Kirchner et al., 2000). For these contaminants, one of the primary modes of transport is driven by the groundwater movement. Zinn et al. (2004) have demonstrated solute transport displaying mass transfer behavior in laboratory experiments designed to visualize solute transport through a thin chamber packed with glass beads and containing circular emplacements of smaller glass beads with lower conductivity, both breakthrough curves and chamber images confirm that different contrasts in small-scale K lead to different regimes of solute transport and thus require different models of upscaled solute transport. Heidari and Li (2014) examine how heterogeneity structure, in particular correlation length, controls flow and solute transport with two-dimensional (2D) sandboxes and four modeling approaches, including 2D Advection-Dispersion Equation (ADE) with explicit heterogeneity structure, 1D ADE with average properties, and nonlocal Continuous Time Random Walk (CTRW) and fractional ADE (fADE). Figuring out the behaviors of solute or contaminant transport in groundwater basins and identifying sources of groundwater contamination, especially within a hierarchically nested flow system, will not only contribute to a deeper understanding of the circulation and evolution of groundwater flow systems, but also help us use the theory of regional groundwater flow to resolve solute or contaminant loading issues in basins.

During the research, considering the large-scale nature of regional hydrogeology, it is very difficult and consuming to conduct field experiments. Instead, methods of analytical and numerical simulations are mainly adopted, which make our understanding of the spatial distributions of groundwater age in drainage basins (Han et al., 2014; Jiang et al., 2010, 2012; Xie et al., 2022) and the residence time distributions (RTDs) for the topography-driven Tóth problem more profound (Basu et al., 2012; Cardenas, 2007; Cardenas and Jiang, 2010; Gusyev et al., 2013; Maxwell et al., 2016; Wang et al., 2016; Wörman et al., 2007). In contrast, although it is confirmed that the physical model experiment can help us understand solute transport through direct observations (Simpson et al., 2003), however, up to now, to our knowledge, experiments regarding solute transport within a hierarchically nested flow system have not been found. The use of physical model experiments to characterize the regional groundwater flow systems is so far still limited to complex Flow System Sand-Box Model of Liang et al. (2010), which only has to do with the groundwater movement, and no solute transport is involved. By making modifications to the physical instrument and adding the solute transport simulation capabilities, it is plausible to carry out the physical solute transport simulation for groundwater flow systems.

In this paper, by modifying the physical instrument of Flow System Sand-Box Model, we simulate solute transport in a Unit basin of a simple flow system and a Tóthian basin of a hierarchically nested flow structure. We first add step-input solutes at recharge zones, separately or simultaneously, within the basin to obtain the breakthrough curves at each recharge zone, and then indirectly obtain the pulse-input breakthrough curves, which are equivalent to the residence time distributions (RTDs). In the end, the self-purification experiments are conducted by inputting water into the basin after the solute-input experiments.

2. Methods

2.1. Structure and function of the instrument

The physical instrument used in this study is an improved version of the Flow System Sand-Box Model developed by Liang et al. (2010). Physically, it consists of three parts: the solute input system, the physical simulation system, and the monitoring system (Fig. 1). The main function of the solute input system is to uniformly input the solutes into the physical simulation system. It is composed of a water supply tank, a peristaltic pump, rubber hoses, and an input device. The water supply tank can store and provide pre-prepared solutes. The peristaltic pump transfers the solutes from the water supply tank into the input device through rubber hoses. It should be noted that the peristaltic pump used in the current experiment has a capacity ranging from 0.0001 to 720 mL/min. By adjusting the flow rate, we can have different solute-input intensities, thus simulating groundwater flow systems of different flow patterns with three step-down-located drainage ports. The input device is a simple plastic box with uniformly-distributed holes at the bottom, and water flows out through the uniformly-distributed holes to form precipitation. Therefore, solutes introduced by the peristaltic pump can be uniformly input into the physical simulation system.

The physical simulation system is a hierarchical groundwater flow system simulator. Its main function is to simulate and display groundwater flow and solute transport for different flow patterns. The geometry of the physical simulator is as follows: the length is 1.0 m, the thickness is 0.1 m, the height is 0.6 m, and the volume is 0.06 m^3. Three recharge zones, i.e., the upstream recharge zone RZ1, midstream recharge zone RZ2, and downstream recharge zone RZ3, are shown in Fig. 1. In the recharge zones, solutes are uniformly injected by the solute input system mentioned above. Inside the simulator, three step-down-located drainage ports are used to realize the function of discharge zones, i.e., the upstream discharge zone DZ1, midstream discharge zone DZ2, and downstream discharge zone DZ3 (Fig. 1). The physical simulator or the sandbox is filled with homogenous quartz sands. The effects of heterogeneity and anisotropy properties of aquifers will be further considered in the future. It should be noted that at the top of the simulator in each recharge zone, a row of rubber tips is placed (Fig. 1). Red ink can be injected by the rubber tips to trace groundwater flow pathways.

The monitoring system consists of a drainage tank, a waste water tank, and an electrical conductivity monitoring system. The drainage tank is used to receive water discharged from each drainage port. The electrical conductivity probes are placed in the drainage tank to collect electrical conductivity data, which can be converted into solute concentrations by empirical equations. An electrical conductivity display panel can display the real-time electrical conductivity and its time-varying curves. The waste water tank is used to store the waste water from the drainage tank. The electrical conductivity probes have a capacity of 0.02–20 ms/cm and a monitoring frequency of 6 s. Flow rates

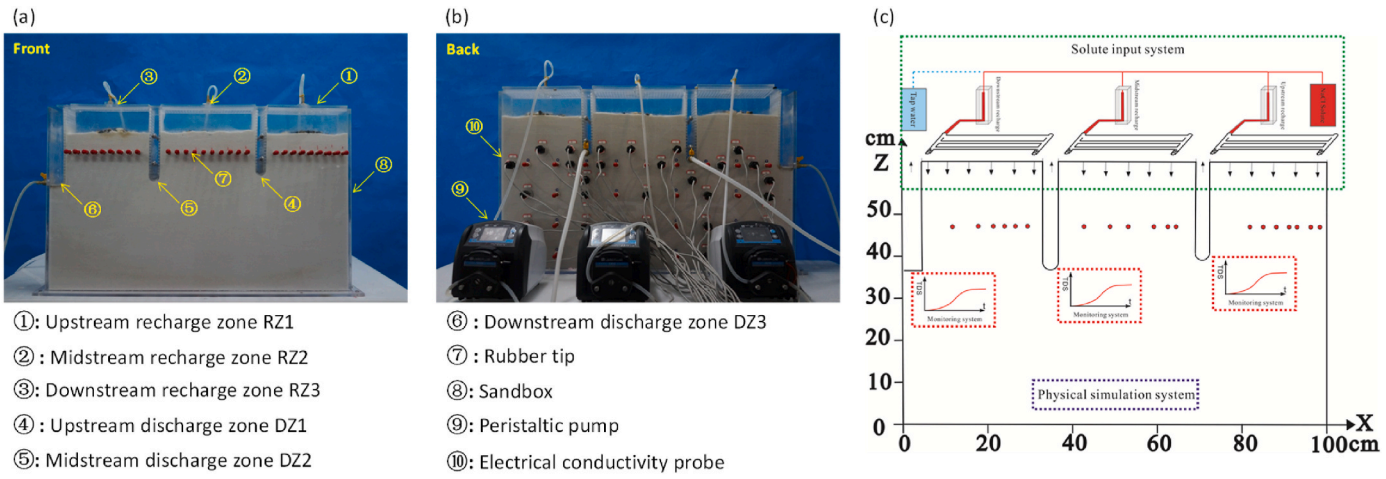

Fig. 1. Configuration of the modified physical instrument of Flow System Sand-Box Model. (a) The front-image, (b) back-image, and (c) schematic diagram of the physical instrument.

in each discharge zone are measured by using a measuring cup and a stopwatch.

2.2. Groundwater flow system

After assembling the physical instrument or the sandbox, we can simulate groundwater flow systems of different flow patterns. We inject the red ink by using the rubber tips for groundwater pathway tracing. When all the injected red ink finally converges at the DZ3 showing a simple one-cell flow field, a unit basin of a flow system can be established (Fig. 2a and b). Comparatively, when all the red ink converges at three different discharge zones showing a nested flow pattern, and all the three discharge zones have water flowing out, in particular, the DZ2 has flow lines from the RZ1, a Tóthian basin of a hierarchical groundwater flow system can be established (Fig. 2c and d). We record the flow rate of peristaltic pumps at each recharge zone to serve for the following solute transport experiments, and monitor the recharge intensity and discharge intensity to calculate water balance.

2.3. Solute transport

Solutes injecting into the groundwater basin generally can be summarized in two ways, i.e., the step-input and the pulse-input. For a step-input injection, its breakthrough curve is equivalent to the cumulative residence time distribution (CRTD), and its time derivative is equivalent to the residence time distribution (RTD). For a pulse-input injection, mathematically, its breakthrough curve is just the residence time distribution (RTD) (Cardenas et al., 2008; Cardenas, 2007; Cornaton and Perrochet, 2006). Therefore, in theory, the step-input and the pulse-input methods can be interconverted under certain circumstances.

To ensure the experiment operation's convenience and data quality, we choose a step-input method to obtain the breakthrough curve. The

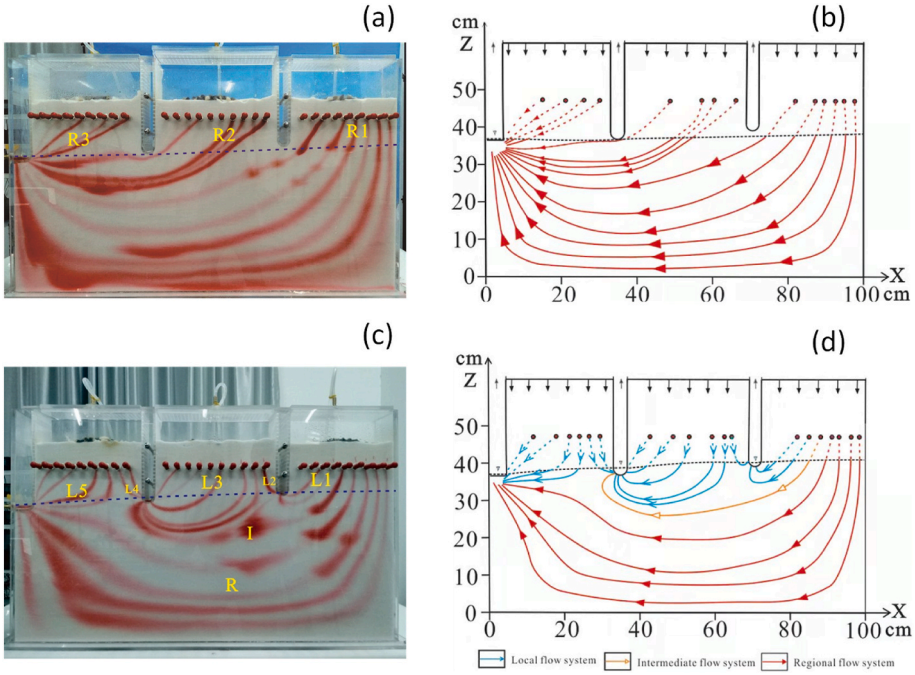

Fig. 2. Flow fields of (a, b) the Unit basin of a simple flow system and (c, d) the Tóthian basin of a hierarchically nested flow system traced by the red ink. (a, c) Pictures of the experiment; (c, b) interpretation of the observed flow system. Here, R denotes Regional flow system, I is Intermediate flow system and L stands for Local flow system. (For interpretation of the references to colour in this figure legend, the reader is referred to the Web version of this article.)

NaCl solute with a concentration of $C_0 = 1126$ mg/L is continuously and stably injected into the recharge zones from the time $t = 0$. To be more general, results are normalized by using Equations (1) and (2):

$$t^* = \frac{t}{T_c} = \frac{tQ}{V} \quad \text{(Equation 1)}$$

where t^* is the normalized time, t is the time, T_c is the characteristic residence time defined as the ratio of the basin volume V to the total recharge Q. For this experiment, the basin volume is 0.006 m^3, and the recharge rate is 0.62 mL/s for the unit basin, and 3.55 mL/s for the Tóthian basin (Table 1), respectively. Therefore, the characteristic residence time for the unit basin is about 27 h, and for the Tóthian basin is about 4.7 h.

For the solute concentration, we introduce

$$C^* = \frac{C - C_{tw}}{C_0 - C_{tw}} \quad \text{(Equation 2)}$$

where C^* is the normalized concentration, C is the solute concentration, C_0 is the concentration of the solute injected at the recharge zones, C_{tw} is the concentration of the tap water.

In the experiment, two kinds of solutes are used. One is tap water with an electrical conductivity of 305 μs/cm, which represents the background concentration. The other is the NaCl solute with an electrical conductivity of 2000 μs/cm, which represents the solutes or contaminations. The NaCl solute is selected by only considering convection and diffusion. Solutes that are not conservative or have properties such as reactions will be considered in the future.

During the experiment, concentrations of the solute are indirectly measured by the electrical conductivity probes. Following common procedures, we prepare NaCl solutions of different concentrations in the lab and then measure their electrical conductivity values using the probe. The conversion from electrical conductivity to concentration is established in the lab by the linear regression of experimental data as

$$C = 0.564 \cdot EC - 2.168 \quad \text{(Equation 3)}$$

where C is the solute concentration in mg/L, EC is the electrical conductivity in μs/cm. In terms of concentration, the tap water is approximately 170 mg/L and the NaCl solution is approximately 1126 mg/L.

3. Results

3.1. Flow system

3.1.1. Unit basin

As can be seen from Fig. 2a and b, with recharge intensities of 0.23, 0.17 and 0.22 mL/s at the RZ1, RZ2 and RZ3, respectively (Table 1), the basin develops only a flow system with a homogeneous circulation, and all the recharged groundwater finally discharges at the most downstream DZ3. More specifically, the red ink tracing pathways indicates that groundwater recharged from the RZ1 flows through the bottom of the basin to discharge at the DZ3, forming a most distant and deepest regional-like flow system. Groundwater recharged from the RZ2 flows through the middle part of the basin to discharge at the DZ3, forming an intermediate-like flow system. Groundwater recharged from the RZ3 flows through the shallow part of the basin to discharge at the DZ3, forming a short and shallow local-like flow system. The discharge intensity at the DZ3 is approximately 0.62 mL/s, which is equal to the total recharge intensity of the recharge zones. This indicates that the flow field has reached a stable water balance state.

Table 1
Recharge and discharge intensities in the Unit basin and the Tóthian basin.

Flow system	Recharge/ Discharge zone	Upstream	Midstream	Downstream	Total
		mL/s	mL/s	mL/s	mL/s
Unit basin	Recharge zone	0.23	0.17	0.22	0.62
	Discharge zone			0.62	0.62
Tóthian basin	Recharge zone	1.71	1.16	0.68	3.55
	Discharge zone	0.83	1.32	1.40	3.55

3.1.2. Tóthian basin

In a Tóthian basin, as shown in Fig. 2c and d, it develops a hierarchically nested flow system when the recharge intensity at the RZ1, RZ2, and RZ3 is 1.71, 1.16, and 0.68 mL/s, respectively (Table 1). More specifically, groundwater recharged from the RZ1 flows to the DZ1, DZ2, and DZ3, leading to the development of local flow system L1, intermediate flow system I, and regional flow system R. Groundwater recharged from the RZ2 flows to the DZ1 and DZ2, leading to the development of local flow systems L2 and L3. Groundwater recharged from the RZ3 flows to the DZ2 and DZ3, leading to the development of local flow systems L4 and L5. The discharge rate at the DZ1, DZ2, and DZ3 is 0.83, 1.32, and 1.40 mL/s, respectively, whose total amount is consistent with the total recharge. A steady state and a good water balance are shown.

3.2. Step-input solute transport

3.2.1. Unit basin

Step-input solute transport in the unit basin is shown in Fig. 3a. After injected into the groundwater basin at the three recharge zones simultaneously, the solute transports under the driving force of groundwater flow. Because it is a simple flow system of one flow cell, only the downstream DZ3 has groundwater flowing out, and only the electrical conductivity probe in the DZ3 has a response (Fig. 3a). With time increasing, the breakthrough curve of the unit basin shows a gradual upward trend with a decreasing slope, from a concentration value of $C^* = 0$ to $C^* = 1.0$, and remains relatively stable, indicating that the entire groundwater basin is gradually filled with contaminated solutes.

Compared to the breakthrough curves for a unit basin shown in the literature (Cardenas, 2007; Wang et al., 2016), two more pronounced steps, which approximately correspond to normalized concentration values of 0.35 and 0.6, respectively, are observed in the current experiment. This phenomenon is caused by the settings of the current physical instrument. In the physical instrument, the solute is not input across the entire water table as those shown in Cardenas (2007) and Wang et al. (2016). More specifically, no solutes are input at the upper two discharge ports DZ1 and DZ2. Because the DZ1 and DZ2 occupy a relatively large proportion of the entire water table, two discrete behaviors will be shown in the flow system, resulting in the existence of the two obvious steps. In practice, the precipitation recharge within the basin is often uneven-spatially distributed, and the precipitation intensity may also vary a lot with space, which can eventually lead to the presence of internal steps in the breakthrough curves.

3.2.2. Tóthian basin

Driven by the hierarchically nested flow structure, breakthrough curves of the Tóthian basin would show quite different behaviors when solutes are input at different recharge zones. In the solute transport experiments, we set three scenarios: I) solutes are simultaneously input at the three recharge zones; II) solutes are input at the up-, mid-, and down-stream recharge zones, respectively; III) solutes are simultaneously input at two of the three recharge zones, respectively. These three scenarios are the most common ones in nature and are of important hydrological significance.

Since the groundwater basin is a linear system, Scenario II is the basic benchmark. Theoretically, Scenario I and Scenario III can be reproduced by superposing the three breakthrough curves of the DZ1, DZ2, and DZ3 of Scenario II. Here, we introduce the Scenario I and the Scenario II in details (Figs. 3 and 4). For Scenario III, we show the results in the Supplementary Material (Fig. S1).

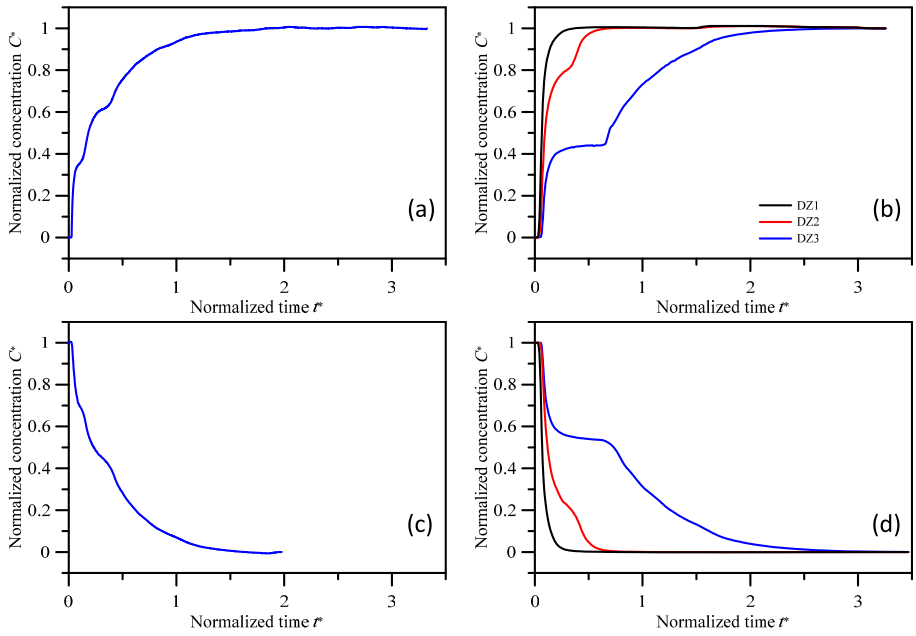

Fig. 3. Step-input breakthrough curves for (a) the unit basin and (b) the Tóthian basin. Here, solutes are input at the three recharge zones simultaneously. Self-purification breakthrough curves for (c) the unit basin and (d) the Tóthian basin. Here, tap water is input at the three recharge zones simultaneously.

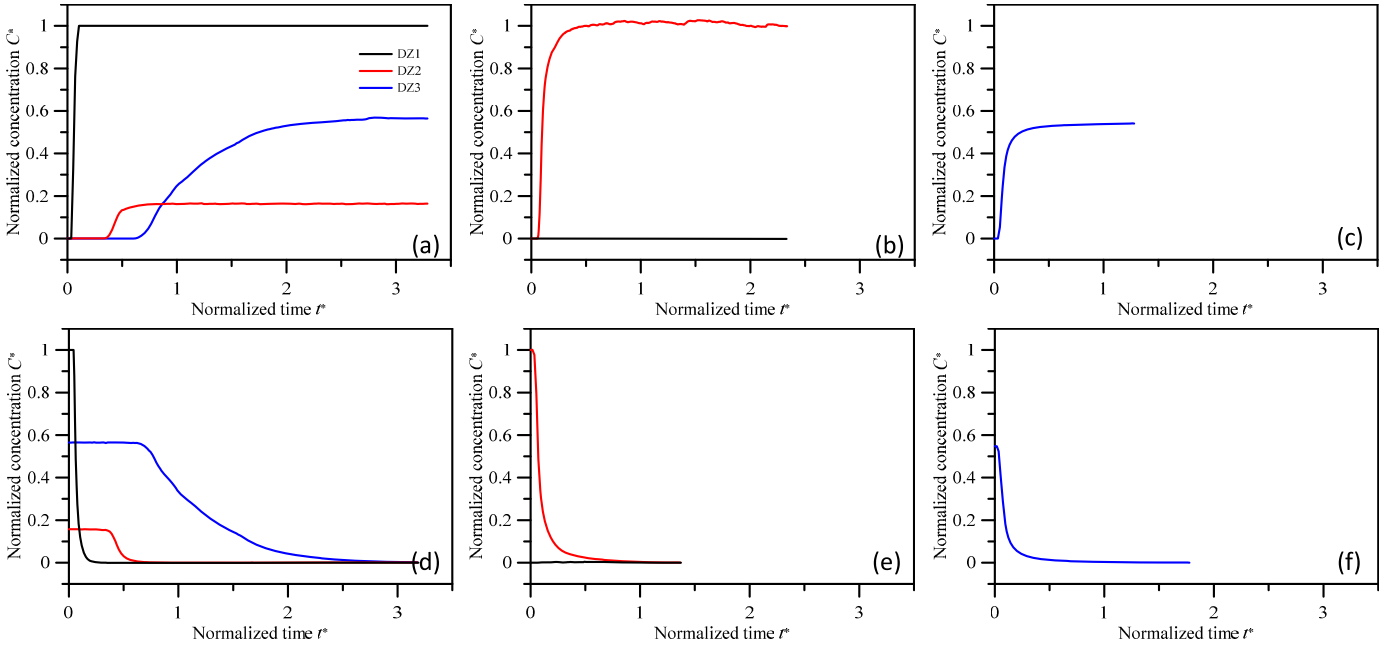

Fig. 4. Breakthrough curves for solute separately input at each recharge zone in Tóthian basin: solute is input only at (a) the upstream RZ1, (b) the midstream RZ2, and (c) the downstream RZ3. Self-purification breakthrough curves for tap water input at each recharge zone: tap water is input only at (d) the upstream RZ1, (e) the midstream RZ2, and (f) the downstream RZ3.

3.2.2.1. Solute-input at three recharge zones. In the Tóthian basin, driven by the hierarchically nested flow structure, all three discharge zones will have a response when solutes are simultaneously input at the three recharge zones (Fig. 3b). The breakthrough curve in the upstream DZ1 has only one upward trend, with the solute concentration rising rapidly from a concentration value of $C^* = 0$ and stabilizing at $C^* = 1.0$. The upstream DZ1 receives recharge both from local flow systems L1 and L2. As these two local flow systems do not differ significantly in their degrees of development, this breakthrough curve does not exhibit a discrete behavior at time scale.

In contrast to the DZ1, the breakthrough curve of the DZ2 has two upward trends and a transitory internal step. As indicated by the flow

field, the first upward trend is caused by the solutes from the local flow systems L3 and L4, and the second upward trend by the solutes from the intermediate flow system I. The starting point of the second upward trend approximately corresponds to a time of $t^* = 0.35$, indicating that the characteristic residence time of the intermediate flow system I is about $t^* = 0.35$. In other words, the intermediate flow system recharged from the RZ1 will take about $t^* = 0.35$ to finally discharge at the DZ2. The internal step maintains at the concentration value of $C^* = 0.8$ with a life of $t^* = 0.05$. This indicates that the arrival of the intermediate flow system is about $t^* = 0.05$ later than the residence time of the two local flow systems. Moreover, it should be noted that the slope of the second upward trend is a little smaller than the first. This is because the flow velocity or the solute transport in the intermediate flow system is slower than that of the local flow systems.

Similar to the DZ2, the breakthrough curve of the DZ3 also has two upward trends and one internal step. As indicated by the flow field, the first upward trend represents the solutes from the local flow system L5, and the second upward trend represents the solutes from the regional flow system R. The starting point of the second upward trend approximately corresponds to a time of $t^* = 0.65$, indicating that the characteristic residence time of the regional flow system R is $t^* = 0.65$, and that groundwater recharged from the RZ1 will take about $t^* = 0.65$ normalized time to finally discharge at the DZ3. The internal step is sustainable and maintains the concentration value of $C^* = 0.55$ with a life of $t^* = 0.4$. This indicates that the arrival of regional flow system R is about $t^* = 0.4$ later than that of the local flow system L5. Moreover, it should be noted that the slope of the second upward trend is much smaller than the first. This is because the flow velocity or the solute transport in the regional flow system is much slower than that of the local flow system.

Compared to the DZ2, the internal step of the DZ3 is much more persistent and the slope of the second upward trend of the DZ3 is much smaller. This is since the regional flow system R has a longer pathway length and a slower flow velocity than the intermediate flow system I, and that a longer residence time will take to finally discharge.

3.2.2.2. Separately solute-input at each recharge zone

3.2.2.2.1. Separately solute input at the upstream RZ1.

For the scenario that solute is input only at the upstream RZ1, driven by the hierarchically nested flow structure, all three discharge zones have a response (Fig. 4a). Specifically, the upstream DZ1 responds rapidly from a concentration value of $C^* = 0$ and finally stabilizes at about $C^* = 1.0$ within a relatively short time. As indicated by the flow field, the DZ1 receives groundwater both from the local flow systems L1 and L2, but its solute is only from the local flow system L1. Since the final step of the breakthrough curve is close to $C^* = 1.0$, it shows that the contribution of the local flow system L2 to the DZ1 is not significant.

When $t^* = 0.35$, the breakthrough curve of the DZ2 begins to respond, rises up rapidly, and finally stabilizes at a concentration value of $C^* = 0.18$. As indicated by the flow field, the DZ2 receives groundwater both from the local flow systems L3, L4, and the intermediate flow system I, but its solute is only from the intermediate flow system I. The final step of the breakthrough curve is about $C^* = 0.18$, indicating that the contribution of the intermediate flow system I to the DZ2 is limited.

When $t^* = 0.65$, the breakthrough curve of the DZ3 begins to respond, rises up tenderly, and finally stabilizes at a concentration value of $C^* = 0.55$. As indicated by the flow field, the DZ3 receives groundwater both from the local flow systems L5 and the regional groundwater flow R, but its solutes are only from the regional flow system R. The final step of the breakthrough curve is about $C^* = 0.55$, indicating that the contribution of the regional flow system R to the DZ3 is significant.

3.2.2.2.2. Separately solute-input at the midstream RZ2.

For the scenario that solutes are input only at the midstream RZ2, driven by the hierarchically nested flow structure, theoretically, the midstream DZ2 and the upstream DZ1 should have a response. However, in the current experiment, only the electric conductivity probe in the DZ2 has a strong response, which increases rapidly from a concentration value of $C^* = 0$ and finally stabilizes at $C^* = 1$ within a very short time. The electric conductivity probe in the DZ1, in contrast, almost has no response (Fig. 4b). As indicated by the flow field, although the DZ1 receives groundwater both from the local flow systems L1 and L2, it only receives solutes from the local flow system L2. This phenomenon implies that the contribution of the local flow system L2 to the DZ1 is tiny.

3.2.2.2.3. Separately solute input at the downstream RZ3.

For the scenario that solutes are input only at the downstream RZ3, driven by the hierarchically nested flow structure, only the downstream DZ3 responds significantly. The upstream DZ1 and midstream DZ2 have little or no response within the monitoring range of the instrument (Fig. 4c). Specifically, the breakthrough curve of the DZ3 responds rapidly from a concentration value of $C^* = 0$ and finally stabilizes at about $C^* = 0.55$. As indicated by the flow field, the DZ3 receives groundwater both from the local flow system L5 and the regional flow system R, but its solute only comes from the local flow system L5. This phenomenon implies that the contribution of the regional water flow system from the deep circulation to the DZ3 is significant, and should not be neglected in the analysis of water balance, especially for study areas located at downstream of a basin.

3.2.2.3. Circulation rate for each flow system.

For a Tóthian basin of a hierarchically nested flow system, characterizing the circulation behaviors of each flow system is the key to using the theory of regional groundwater flow (Tóth, 2009) to analyze and solve practical hydrogeologic problems. Following the principle of water mass balance, and taking circulation rates of each flow system as variables, we can set up 7 water mass balance equations. Specifically, for the recharge zones, we can have

$$\text{Recharge zone 1}: V_{L1} + V_I + V_R = V_{RZ1} \quad \text{(Equation 4–1)}$$

$$\text{Recharge zone 2}: V_{L3} + V_{L2} = V_{RZ2} \quad \text{(Equation 4–2)}$$

$$\text{Recharge zone 3}: V_{L5} + V_{L4} = V_{RZ3} \quad \text{(Equation 4–3)}$$

for the discharge zones, we can have

$$\text{Discharge zone 1}: V_{L1} + V_{L2} = V_{DZ1} \quad \text{(Equation 4-4)}$$

$$\text{Discharge zone 2}: V_{L3} + V_{L4} + V_I = V_{DZ2} \quad \text{(Equation 4–5)}$$

$$\text{Discharge zone 3}: V_{L5} + V_R = V_{DZ3} \quad \text{(Equation 4–6)}$$

Note that the recharge rates should be equal to the discharge rates

$$V_{DZ1} + V_{DZ2} + V_{DZ3} = V_{RZ1} + V_{RZ2} + V_{RZ3} \quad \text{(Equation 4–7)}$$

In the above equations, 7 unknown variables are all listed. Namely, V_{L1}, V_{L2}, V_{L3}, V_{L4}, V_{L5} are the unknown circulation rates for local flow systems L1 to L5; V_I is the unknown circulation rate for the intermediate flow systems I; V_R is the unknown circulation rate for the regional flow system R. In contrast, V_{RZ1}, V_{RZ2}, V_{RZ3} of the recharge intensities for the recharge zones RZ1 to RZ3 and V_{DZ1}, V_{DZ2}, V_{DZ3} of the discharge intensities for the discharge zones DZ1 to DZ3 are known quantities. They can be measured or controlled during the solute transport experiment.

In Equation 4, for the 7 unknown variables, only 6 effective water mass balance equations (Equations 4-1-4-6) are set up. In order to obtain a unique solution, more equations are needed. The current solute transport experiment is just in time to provide help. After knowing the mode of flow structure, by using the internal steps of the breakthrough curves to identify the intermediate and regional flow systems, we can set up two more solute mass balance equations. By jointly solving them with the water mass balance equations, the circulation rate for each flow system can be calculated.

Here, we just introduce the Scenario I as an example. For other scenarios, since the basic principles are the same, we can use the same

method to calculate the circulation rate for each flow system. In Fig. 3b, the internal step in the breakthrough curve of DZ2 implies that the solute from the intermediate flow system I has not been discharged at the DZ2, and that the solute in the DZ2 is only contributed by the local flow systems L3 and L4. Therefore, the solute mass balance equation can be set up as follows:

$$\frac{V_{L3}+V_{L4}}{V_{L3}+V_{L4}+V_I}=0.8 \quad \text{(Equation 5–1)}$$

Similarly, in Fig. 3b, the internal step in the breakthrough curve of DZ3 implies that the solute from the regional flow system R has not been discharged at the DZ3, and that the solute in the DZ3 is only contributed by the local flow system L5. Therefore, the solute mass balance equation can be set up as follows:

$$\frac{V_{L5}}{V_{L5}+V_R}=0.45 \quad \text{(Equation 5–2)}$$

By jointly solving Equations 4 and 5, the circulation rate for each flow system shows that, in the current experiment, the circulation rate for the local flow system L1 is 0.676 mL/s, for the local flow system L2 is 0.154 mL/s, for the local flow system L3 is 1.006 mL/s, for the local flow system L4 is 0.05 mL/s, for the local flow system L5 is 0.63 mL/s, for the intermediate flow system I is 0.264 mL/s, and for the regional flow system R is 0.77 mL/s. The circulation rate for each flow system quantitatively explains the experimental phenomena. For example, the contribution of the local flow system L2 to the DZ1 is tiny, the contribution of the intermediate flow system I to the DZ2 is limited, and the contribution of the regional flow system R to the DZ3 is dominant.

4. Discussions

4.1. Pulse-input solute transport

By deriving the step-input breakthrough curve respective to time t, we can equivalently obtain the pulse-input breakthrough curve, which is also the residence time distribution of the groundwater basin (Cardenas et al., 2008; Cardenas, 2007; Cornaton and Perrochet, 2006). Here, we only discuss Scenario I (Fig. 5). For other Scenarios, we have plotted the pulse-input breakthrough curves, which can be referred to the Supplementary Material (Figures S2~S3). In general, the step-input breakthrough curve is characterized by upward trends and internal steps (Figs. 3–4), while that of a pulse-input injection is characterized by peaks and sloping tails (Fig. 5).

4.1.1. Unit basin

For the unit basin, we plot the pulse-input breakthrough curve or the residence time distribution by deriving Fig. 3a respective to time t in a logarithmic coordinate system (Fig. 5a). In Fig. 5a, three decreasing peaks with sloping tails can be identified. Among them, the first early-time peak is quite significant. While, due to external interferences, the latter two peaks appear messy, but can still be identified.

The pulse-input breakthrough curve or residence time distribution is different from the results given by previous studies (Cardenas, 2007; Wang et al., 2016, i.e.), two more peaks with sloping tails are observed. The reason for the existence of these two peaks is the same as that explained previously in section 3.2.1. DZ1 and DZ2 occupy a relatively large proportion of the entire water table, but no solutes are input at the two discharge zones.

4.1.2. Tóthian basin

For the Tóthian basin, as the scenario is that solutes are simultaneously input at the three recharge zones, we can superimpose the pulse-input breakthrough curves of the three discharge zones to plot the breakthrough curve or residence time of the entire basin (Fig. 5b). Consistent with the results of previous numerical simulations, driven by the hierarchically nested flow structure, in Fig. 5b, three peaks with sloping tails can be identified. Compared with the unit basin, although the two are the same in the form of three peaks with sloping tails, the causes are completely different. For the Tóthian basin, the flow field indicates that the first early-time peak is due to the early arrival of local flow systems with the shortest residence time, the second mid-time peak is due to the later arrival of the intermediate flow system with a longer residence time, and the late-time peak is due to the final arrival of the regional flow system with the longest residence time. Therefore, when analyzing field observation data regarding the discrete time-scale behaviors of the breakthrough curves, careful attention should be paid. As shown above, peaks with sloping tails can be caused by the heterogeneity of the distribution and intensity of the recharge, or be caused by the nested structure of groundwater flow systems.

4.1.3. Slope of the tail

When analyzing the pulse-input breakthrough curve or residence time distribution, one of the key points we have concerned about is the slope of the descending tail after each peak (Kirchner et al., 2000). The slope indicates the rate at which solutes are flushed out or contaminants fade away. In general, the larger the slope is, the faster the solutes are flushed out, the shorter contaminants reside in the basin, and the easier contaminants are controlled; the smaller the slope is, the slower the solutes are flushed out, the longer contaminants reside in the basin, and the harder contaminants are controlled. For the unit basin, the slopes of the three peaks are the same. This indicates that the flow fluid is homogeneous and the circulation intensity inside the unit basin is the same. For the Tóthian basin of a hierarchically nested flow structure, the slope of the first early-time peak is the largest, and caused by local flow systems; the slope of the second mid-time peak is the intermediated, and caused by the intermediate flow system, the slope of the third late-time peak is the smallest, and caused by the regional flow system. The slopes tell us, that if the local flow system is contaminated, it is relatively easy to be relieved. For the intermediate or regional flow system, if contaminated, they are even more difficult to be relieved. This is consistent with the basic principle of the theory of regional groundwater flow proposed by Tóth (2009).

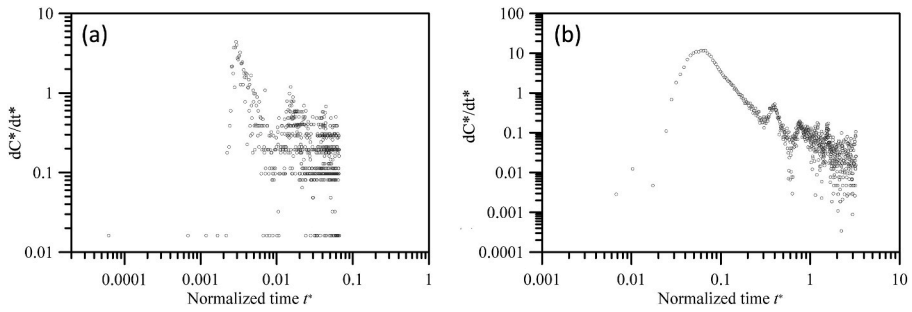

Fig. 5. Pulse-input breakthrough curves or residence time distributions (RTDs) for (a) the unit basin and (b) the Tóthian basin. Here, solutes are input at the three recharge zones simultaneously.

In addition, the monitored residence time in this paper starts from the precipitation begins to seep in, that is, the water flow passes through the vadiscate zone. However, the previous analytical or numerical simulation results only consider the saturated zone, that is, starting from the water table (Wang et al., 2016; Cardenas and Jiang, 2010). Therefore, the results of the physical experiment in this paper are more consistent with the reality. As can be seen from Fig. 5, the data points rise and fall continuously, and the initial low or even constant value corresponds to the influence of the vadose zone. However, the data points of previous studies change abruptly, missing the previous gradually rising segment.

4.2. Self-purification of groundwater flow systems

As groundwater is deeply buried beneath the land surface, the perception of groundwater pollution is always hindsight. In other words, people take measures to shut down the contaminated sources usually after the groundwater is found to be polluted, and then begin to systematically observe the pollution concentration variations. This is in line with the basic theory of Geology-the present and the past, i.e., using the present monitoring data to analyze important geologic historical events that happened in the past. To give a more vivid example, after nuclear explosions in the 1960s, we thought of using Tritium for dating (Suckow, 2014). Therefore, can the monitoring data after the occurrence of pollution be effectively used to analyze the groundwater circulation and the behavior of solute transport in basins? In response to the above question, we continuously carry out the self-purification experiment. That is, we will continuously input tap water into the groundwater basin to purify the contaminations and monitor the concentration variations.

As can be seen from the breakthrough curves (Figs. 3–4, S1), whether it is a simple flow system of one flow cell or a complex flow system of a nested flow structure, whether solutes are simultaneously input at three recharge zones, separately at each recharge zone, or at two of three recharge zones, the shapes of the solute-input curves and the self-purification curves are systematically symmetrical. As the self-purification experiment has less external interference, the shape of the curve is better than that of the solute-input experiment. Therefore, it is entirely possible to consider using the self-purification curves to characterize and identify the groundwater flow system. This is consistent with the idea of using the pumping test recovery data to estimate hydrogeological parameters (Todd and Mays, 2005).

5. Conclusions

In this paper, we modify the physical instrument of Flow System Sand-Box Model by inputting solute in recharge zones and installing high-frequency conductivity monitoring probes in discharge zones, and simulate the solute transport in a Unit basin of a simple flow system and a Tóthian basin of a hierarchically nested flow structure.

For the Unit basin, solutes are step input at the three recharge zones simultaneously. Compared to those reported in the literature, two more pronounced steps are observed, which is caused by the settings of the current physical instrument as no solutes are input at the upper two discharge ports. For the Tóthian basin, driven by the flow field, the breakthrough curves for the Tóthian basin in each discharge zone show a general upward trend, and internal steps may exist due to the late-time arrival of intermediate and regional groundwater flow systems. Although the Unit basin and Tóthian basin can both have steps in the breakthrough curves, they are due to different reasons.

By jointly solving solute mass balance equations with water mass balance equations, the circulation rate for each flow system is calculated, which quantitatively explains the phenomena encountered in the experiment, and highlights the important contributions of intermediate and regional flow system to the entire groundwater circulation.

By deriving the step-input breakthrough curve with respective to time, we equivalently obtain the pulse-input breakthrough curve, which represents the residence time distribution of the groundwater basin. The breakthrough curve of a pulse-input injection is characterized by the peaks and sloping tails. The peaks are caused by the late-time arrival of intermediate and regional groundwater flow systems. The slopes indicate the rate at which solutes are flushed out or contaminants fade away, which tell us that local flow system is relatively easy to be relieved from contamination, while the intermediate or regional flow system is even more difficult to be relieved.

By inputting tap water into the groundwater basin to purify the contaminations, we conduct self-purification experiments. The shapes of the solute-input curves and the self-purification curves are systematically symmetrical. As the self-purification experiment has less external interference, the shape of the curve is better than that of the solute-input experiment. It is entirely possible to consider using the self-purification curves to characterize and identify the groundwater flow system.

CRediT authorship contribution statement

Hong Niu: Conceptualization, Methodology, Experiment, Writing – original draft. **Jun-Zhi Wang:** Conceptualization, Methodology. **Sheng-Nan Ni:** Writing – original draft. **Xing Liang:** Conceptualization, Methodology. **Hong Du:** Data curation.

Declaration of competing interest

No conflict of interest exists in the submission of this manuscript, and all authors are aware of this submission. This manuscript has not been published previously and is not under consideration by another journal or conference proceeding.

This study is financially supported by National Natural Science Foundation of China (41807186, 41902245, 42004071), the Key R&D and Promotion Projects of Henan Province: Scientific Research (212102311150), the Fundamental Research Funds for the Central Universities, South-Central MinZu University (CZY23011). Thanks for the decication of Jun-Chao Gong and Biao Peng during the experiment.

Data availability

The data that has been used is confidential.

Acknowledgments

This study is financially supported by National Natural Science Foundation of China (41807186, 41902245, 42004071), the Key R&D and Promotion Projects of Henan Province: Scientific Research (212102311150), the Fundamental Research Funds for the Central Universities, South-Central MinZu University (CZY23011). Thanks for the dedication of Jun-Chao Gong and Biao Peng during the experiment.

Appendix A. Supplementary data

Supplementary data to this article can be found online at https://doi.org/10.1016/j.jclepro.2023.138832.

References

Alley, W.M., Healy, R.W., LaBaugh, J.W., Reilly, T.E., 2002. Flow and storage in groundwater systems. Science 296 (5575), 1985–1990. https://doi.org/10.1126/science.1067123.

Basu, N.B., Jindal, P., Schilling, K.E., Wolter, C.F., Takle, E.S., 2012. Evaluation of analytical and numerical approaches for the estimation of groundwater travel time distribution. J. Hydrol. 475, 65–73. https://doi.org/10.1016/j.jhydrol.2012.08.052, 0.

Cardenas, B.M., Wilson, J.L., Haggerty, R., 2008. Residence time of bedform-driven hyporheic exchange. Adv. Water Resour. 31 (10), 1382–1386. https://doi.org/10.1016/j.advwatres.2008.07.006.

Cardenas, M.B., 2007. Potential contribution of topography-driven regional groundwater flow to fractal stream chemistry: residence time distribution analysis of Tóth flow. Geophys. Res. Lett. 34 (5), L05403 https://doi.org/10.1029/2006GL029126.

Cardenas, M.B., Jiang, X.W., 2010. Groundwater flow, transport, and residence times through topography-driven basins with exponentially decreasing permeability and porosity. Water Resour. Res. 46 (11), W11538 https://doi.org/10.1029/2010WR009370.

Cornaton, F., Perrochet, P., 2006. Groundwater age, life expectancy and transit time distributions in advective–dispersive systems: 1. Generalized reservoir theory. Adv. Water Resour. 29 (9), 1267–1291. https://doi.org/10.1016/j.advwatres.2005.10.009.

Dai, X., et al., 2021. Understanding topography-driven groundwater flow using fully-coupled surface-water and groundwater modeling. J. Hydrol. 594, 125950 https://doi.org/10.1016/j.jhydrol.2020.125950.

Freeze, R.A., Witherspoon, P.A., 1967. Theoretical analysis of regional groundwater flow: 2. Effect of water-table configuration and subsurface permeability variation. Water Resour. Res. 3 (2), 623–634. https://doi.org/10.1029/WR003i002p00623.

Gusyev, M., et al., 2013. Calibration of a transient transport model to tritium data in streams and simulation of groundwater ages in the western Lake Taupo catchment, New Zealand. Hydrol. Earth Syst. Sci. 17 (3), 1217–1227.

Haitjema, H.M., Mitchell-Bruker, S., 2005. Are water tables a subdued replica of the topography? Ground Water 43 (6), 781–786. https://doi.org/10.1111/j.1745-6584.2005.00090.x.

Han, W.S., Kim, K.-Y., Jung, N.-H., Park, E., Solomon, D.K., 2014. Transport of groundwater, heat, and radiogenic He in topography-driven basins. Ground Water. https://doi.org/10.1111/gwat.12266 n/a-n/a.

Heidari, P., Li, L., 2014. Solute transport in low-heterogeneity sandboxes: the role of correlation length and permeability variance. Water Resour. Res. 50 (10), 8240–8264. https://doi.org/10.1002/2013wr014654Ingebritsen. , S.E., Sanford, W. E., Neuzil, C.E., 2006. Groundwater in geologic processes. Cambridge University Press, Cambridge, U.K.

Jiang, X.W., Wan, L., Cardenas, M.B., Ge, S., Wang, X.S., 2010. Simultaneous rejuvenation and aging of groundwater in basins due to depth-decaying hydraulic conductivity and porosity. Geophys. Res. Lett. 37 (5), L05403 https://doi.org/10.1029/2010GL042387.

Jiang, X.W., et al., 2012. A quantitative study on accumulation of age mass around stagnation points in nested flow systems. Water Resour. Res. 48 (12), W12502 https://doi.org/10.1029/2012wr012509.

Jiang, X.W., Wan, L., Wang, X.S., Ge, S., Liu, J., 2009. Effect of exponential decay in hydraulic conductivity with depth on regional groundwater flow. Geophys. Res. Lett. 36 (24), L24402 https://doi.org/10.1029/2009GL041251.

Jiang, X.W., Wang, X.S., Wan, L., Ge, S., 2011. An analytical study on stagnation points in nested flow systems in basins with depth-decaying hydraulic conductivity. Water Resour. Res. 47 (1), W01512 https://doi.org/10.1029/2010wr009346.

Kirchner, J.W., Feng, X., Neal, C., 2000. Fractal stream chemistry and its implications for contaminant transport in catchments. Nature 403 (6769), 524–527.

Liang, X., Liu, Y., Jin, M., Lu, X., Zhang, R., 2010. Direct observation of complex Tóthian groundwater flow systems in the laboratory. Hydrol. Process. 24 (24), 3568–3573. https://doi.org/10.1002/hyp.7758.

Liang, X., Quan, D., Jin, M., Liu, Y., Zhang, R., 2013. Numerical simulation of groundwater flow patterns using flux as upper boundary. Hydrol. Process. 27 (24), 3475–3483. https://doi.org/10.1002/hyp.9477.

Marklund, L., Wörman, A., 2011. The use of spectral analysis-based exact solutions to characterize topography-controlled groundwater flow. Hydrogeol. J. 19 (8), 1531–1543. https://doi.org/10.1007/s10040-011-0768-4.

Maxwell, R.M., et al., 2016. The imprint of climate and geology on the residence times of groundwater. Geophys. Res. Lett. 43 (2), 701–708. https://doi.org/10.1002/2015gl066916.

Simpson, M.J., Clement, T.P., Gallop, T.A., 2003. Laboratory and numerical investigation of flow and transport near a seepage-face boundary. Ground Water 41 (5), 690–700. https://doi.org/10.1111/j.1745-6584.2003.tb02407.x.

Suckow, A., 2014. The age of groundwater – definitions, models and why we do not need this term. Appl. Geochem. 50, 222–230. https://doi.org/10.1016/j.apgeochem.2014.04.016.

Todd, D., Mays, L., 2005. Groundwater Hydrology. Groundwater Hydrology. Wiley, New York.

Tóth, J., 1963a. A theoretical analysis of groundwater flow in small drainage basins. J. Geophys. Res. 68 (16), 4795–4812.

Tóth, J., 1962. A theory of groundwater motion in small drainage basins in central Alberta, Canada. J. Geophys. Res. 67 (11), 4375–4387. https://doi.org/10.1029/JZ067i011p04375.

Tóth, J., 1963b. A theoretical analysis of groundwater flow in small drainage basins. J. Geophys. Res. 68 (16), 4795–4812. https://doi.org/10.1029/JZ068i016p04795.

Tóth, J., 1980. Cross-formational Gravity-Flow of Groundwater: a Mechanism of the Transport and Accumulation of Petroleum (The Generalized Hydraulic Theory of Petroleum Migration). Problems of petroleum migration, pp. 121–167.

Tóth, J., 1999. Groundwater as a geologic agent: an overview of the causes, processes, and manifestations. Hydrogeol. J. 7 (1), 1–14. https://doi.org/10.1007/s100400050176.

Tóth, J., 2009. Gravitational Systems of Groundwater Flow. Cambridge University Press, New York.

USEPA, 2008. Handbook for Developing Watershed Plans to Restore and Protect Our Waters. United States Environmental Protection Agency, Washington, DC.

Wang, J.Z., et al., 2016. On the use of late-time peaks of residence time distributions for the characterization of hierarchically nested groundwater flow systems. J. Hydrol. 543, 47–58. https://doi.org/10.1016/j.jhydrol.2016.04.034.

Wang, X.S., Jiang, X.W., Wan, L., Ge, S., Li, H., 2011. A new analytical solution of topography-driven flow in a drainage basin with depth-dependent anisotropy of permeability. Water Resour. Res. 47 (9), W09603 https://doi.org/10.1029/2011WR010507.

Wörman, A., Packman, A.I., Marklund, L., Harvey, J.W., Stone, S.H., 2007. Fractal topography and subsurface water flows from fluvial bedforms to the continental shield. Geophys. Res. Lett. 34 (7), L07402 https://doi.org/10.1029/2007gl029426.

Xie, Y., Love, A.J., Simmons, C.T., Costar, A., Wu, J., 2022. Groundwater age persistence in topography-driven groundwater flow over paleohydrogeologic time scales. Geology. https://doi.org/10.1130/g49842.1.

Zhang, X., et al., 2022. Fractal behaviors of hydraulic head and surface runoff of the nested groundwater flow systems in response to rainfall fluctuations. Geophys. Res. Lett., e2021GL093784 https://doi.org/10.1029/2021GL093784 n/a(n/a).

Zhao, K.-Y., et al., 2018. An analytical study on nested flow systems in a Tóthian basin with a periodically changing water table. J. Hydrol. 556 (Suppl. C), 813–823. https://doi.org/10.1016/j.jhydrol.2016.09.051.

Zijl, W., 1999. Scale aspects of groundwater flow and transport systems. Hydrogeol. J. 7 (1), 139–150. https://doi.org/10.1007/s100400050185.

Zinn, B., et al., 2004. Experimental visualization of solute transport and mass transfer processes in two-dimensional conductivity fields with connected regions of high conductivity. Environ. Sci. Technol. 38 (14), 3916–3926.

Zlotnik, V.A., Cardenas, M.B., Toundykov, D., 2011. Effects of multiscale anisotropy on basin and hyporheic groundwater flow. Ground Water 49 (4), 576–583. https://doi.org/10.1111/j.1745-6584.2010.00775.x.

Zlotnik, V.A., Toundykov, D., Cardenas, M.B., 2015. An analytical approach for flow analysis in aquifers with spatially varying top boundary. Ground Water 53 (2), 335–341. https://doi.org/10.1111/gwat.12205.